

(2)

AD-A255 571



OFFICE OF NAVAL RESEARCH

Contract NOOO14-92J-1590

Technical Report No. CWRU/DMS/TR-46

DTIC
ELECTE
SEP 17 1992
S C D

Theoretical Development for Depth Profiling
of Stratified Layers using Variable Angle ATR

by

Robert A. Shick, Jack L. Koenig and Hatuso Ishida

Department of Macromolecular Science
Case Western Reserve University
Cleveland, Ohio 44106-7202

September, 1992

Reproduction in whole or in part is permitted
for any purpose of the United States Government

This document has been approved for public release and sale;
its distribution is unlimited

Principal Investigator
Hatsuo Ishida
(216) 368-4285

SECURITY CLASSIFICATION OF THIS PAGE

REPORT DOCUMENTATION PAGE

1a REPORT SECURITY CLASSIFICATION None		1b RESTRICTIVE MARKINGS None										
2a SECURITY CLASSIFICATION AUTHORITY None		3. DISTRIBUTION/AVAILABILITY OF REPORT This document has been approved for public release and sale; its distribution is unlimited										
2b DECLASSIFICATION/DOWNGRADING SCHEDULE None		5. MONITORING ORGANIZATION REPORT NUMBER(S) N00014-92J-1590										
4. PERFORMING ORGANIZATION REPORT NUMBER(S) CWRU/DMS/TR - 46		6a NAME OF PERFORMING ORGANIZATION Case Western Reserve University										
6b OFFICE SYMBOL (if applicable)		7a NAME OF MONITORING ORGANIZATION Office of Naval Research										
6c ADDRESS (City, State, and ZIP Code) Department of Macromolecular Science Cleveland, Ohio 44106-1712		7b ADDRESS (City, State, and ZIP Code) 800 North Quincy St. Arlington, VA 22217										
8a NAME OF FUNDING/SPONSORING ORGANIZATION Office of Naval Research		9. PROCUREMENT INSTRUMENT IDENTIFICATION NUMBER										
8b OFFICE SYMBOL (if applicable)		10. SOURCE OF FUNDING NUMBERS										
8c ADDRESS (City, State, and ZIP Code) 800 North Quincy Street Arlington, VA 22217		PROGRAM ELEMENT NO.	PROJECT NO.									
11. TITLE (Include Security Classification) Theoretical Development for Depth Profiling of Stratified Layers using Variable Angle ATR		TASK NO.	WORK UNIT ACCESSION NO.									
12. PERSONAL AUTHOR(S) Robert A. Shick, Jack L. Koenig, Hatsuo Ishida		13a. TYPE OF REPORT Technical Report										
13b. TIME COVERED FROM _____ TO _____		14. DATE OF REPORT (Year, Month, Day) September 11, 1992										
15. PAGE COUNT		16. SUPPLEMENTARY NOTATION Submitted to Applied Spectroscopy										
17. COSATI CODES <table border="1"><tr><th>FIELD</th><th>GROUP</th><th>SUB-GROUP</th></tr><tr><td> </td><td> </td><td> </td></tr><tr><td> </td><td> </td><td> </td></tr></table>		FIELD	GROUP	SUB-GROUP							18. SUBJECT TERMS (Continue on reverse if necessary and identify by block number)	
FIELD	GROUP	SUB-GROUP										
19. ABSTRACT (Continue on reverse if necessary and identify by block number) The theory allowing depth profile information to be recovered from variable angle attenuated total reflection spectroscopy is shown for both perpendicular and parallel polarizations. The errors invoked by the necessary approximations are evaluated by comparison with exact optical simulations using dispersion theory.		20. DISTRIBUTION/AVAILABILITY OF ABSTRACT <input checked="" type="checkbox"/> UNCLASSIFIED/UNLIMITED <input type="checkbox"/> SAME AS RPT. <input type="checkbox"/> DTIC USERS										
21. ABSTRACT SECURITY CLASSIFICATION Unclassified		22a. NAME OF RESPONSIBLE INDIVIDUAL Dr. Kenneth Wynne										
22b. TELEPHONE (include Area Code) (202) 696-4410		22c. OFFICE SYMBOL										

Theoretical Development for Depth Profiling of Stratified Layers using Variable Angle ATR

Robert A. Shick, Jack L. Koenig and Hatsuo Ishida

Department of Macromolecular Science

Case Western Reserve University

Cleveland, Ohio 44106

Accession For	1991-02-01
Spec. File	1
Received Date	1/22/91
Implementation	1
By	
Distribution	
Available in Other	
Serial and/or	
Dist. Serial	
A-1	
DTC QUALITY INSPECTED 3	

Abstract:

The theory allowing depth profile information to be recovered from variable angle attenuated total reflection spectroscopy is shown for both perpendicular and parallel polarizations. The errors invoked by the necessary approximations are evaluated by comparison with exact optical simulations using dispersion theory.

Introduction:

It is often desirable to have molecular information as a function of thickness within a sample. Such information can disclose the details of concentration gradients which would be of interest in a broad number of systems including polymer blends, polymer composites, and coatings. However, the recovery of the profile distribution is not straightforward. One method which will yield this information with proper treatment is variable angle attenuated total reflection Fourier transform infrared spectroscopy (VA-ATR FTIR). In fact, any system which contains gradients as a function of depth could potentially benefit. This method allows the determination of concentration profiles as a function of depth within a sample without disrupting the sample. Currently, it is quite difficult to determine molecular gradient information in the micron size range, and an invasive technique is often used. However, even with proper treatment



87/92

this optical method must be applied judiciously with proper regard to the restraints imposed by the optical constants of the materials involved. It is the intent of this paper to detail the necessary theory to recover the extinction coefficient as a function of depth for stratified layers. There are certain approximations which must be made, specifically that of the extinction coefficient being not too large, and this rather loose criterion is explored more rigorously. The beam intensity is reduced both by the exponential decay of the evanescent wave and absorption. These two effects can be decoupled when absorption is not the dominant effect.

The governing principles of ATR have long been established. Harrick¹ was one of the pioneers in this field and he demonstrated that, above the critical angle required for internal reflection in a layered system, the field intensity in the second medium decays exponentially from the surface of the optically dense material. Generally, it can be said that as the angle of incidence approaches the critical angle, the field strength in the second medium is increased, thereby probing to an increasing depth. In addition, this depth depends on the wavelength of incident radiation. A precise description of the field decay is known which includes the angle of incidence as an operable variable, as well as the refractive indices of the layers and the wavelength of the incident light. As the angle of incidence is changed, the field intensity is also changed, but any profile information at an individual depth is obscured by previous layers in an additive fashion. This difficulty may be overcome by applying inverse Laplace transform mathematics. Since infrared radiation is being employed, it is then possible to obtain vibrational spectroscopic information as a function of depth within the sample.

Theory:

By definition, the sum of the transmittance (T), reflectance (R), and absorptance (A) is equal to unity.

$$T + R + A = 1 \quad (1)$$

The intensity decrease due to reflection occurs when the light impinges on the optically dense material. Radiation impinging on the interface between the incident media and the substrate is either reflected or transmitted. Here the initial transmitted component, T^0 , is equal to $1 - R$. It is commonly known that the field decay within the substrate is exponential above the critical angle.² The configuration under consideration is shown in Figure 1, where the incident media is of higher refractive index than the substrate, and is transparent throughout the frequency range under consideration. Snell's law is applicable for determining the angle of refraction.³

$$n_1 \sin \theta_1 = \hat{n}_2 \sin \hat{\theta}_2 \quad (2)$$

Here, the " \wedge " indicates a complex quantity, where $\hat{n}_2 = n_2 + i k_2$, k being the extinction coefficient, and $i = \sqrt{-1}$. The critical angle, in terms of the incident beam θ_1 , is determined when θ_2 becomes 90° . Therefore, total internal reflection is observed for transparent media when the incident angle is above θ_c .

$$\theta_c = \sin^{-1} \left(\frac{n_2}{n_1} \right) \quad (3)$$

For this condition, the transmittance is actually a function of z and decays exponentially as shown in the following equations:^{3,4}

$$T(z) = T^0 e^{-2\gamma z} \quad (4)$$

$$A(z) = T^0 - T(z) = T^0 (1 - e^{-2\gamma z}) \quad (5)$$

where z is in the depth direction away from the interface between the optically dense material and into the substrate, and γ , the decay coefficient, is shown in the following equation.³

$$\gamma = \frac{2\pi n_1 \operatorname{Im}[\hat{n}_2 \cos \hat{\theta}_2]}{\lambda} \quad (6)$$

The total absorptance, A , is mathematically equal to the sum of $A(z)$ and $T(z)$, and it has the proper limiting condition for non-absorbing substrates, as z approaches infinity the transmitted component approaches zero, and since T^0 is zero, the reflectance goes to 1, which is the case for total internal reflection. Similarly, for absorbing substrates, the absorptance is appropriate because the absorption is zero when the depth is zero, but there is still a field component in the

second medium. For the case of internal reflection, the transmitted component is always zero, except for the case of optical tunnelling, therefore the only loss of reflection is due to absorptance so $R = 1 - [A(z) + T(z)]$, i.e. $R = 1 - A$. The wavelength of the radiation under consideration is given by λ , and "Im" indicates "imaginary part of." The term T^0 is the transmittance at $z=0$, and is dependent on the state of polarization.⁵

$$T_p^0 = \frac{\text{Re}[\hat{n}_2^* \cos \hat{\theta}_2]}{n_1 \cos \theta_1} |\hat{t}_p|^2 \quad (7)$$

$$T_s^0 = \frac{\text{Re}[\hat{n}_2^* \cos \hat{\theta}_2]}{n_1 \cos \theta_1} |\hat{t}_s|^2 \quad (8)$$

The "*" indicates the complex conjugate and "Re" indicates "real part of." Here, the polarization convention follows that s-polarization is for electric field vectors perpendicular to the plane defined by the incident and reflecting beam, and p-polarization is for electric field vectors within that plane. The quantity \hat{t}_p is the complex Fresnel transmission coefficient for p polarization, with an analogous term for s polarization.⁶

$$\hat{t}_p = \frac{2n_1 \cos \theta_1}{\hat{n}_2 \cos \theta_1 + n_1 \cos \hat{\theta}_2} \quad (9)$$

$$\hat{t}_s = \frac{2n_1 \cos \theta_1}{n_1 \cos \theta_1 + \hat{n}_2 \cos \hat{\theta}_2} \quad (10)$$

The following integral relation is valid:

$$\int_0^x e^{-2\gamma z} dz = \frac{1}{2\gamma} (1 - e^{-2\gamma x}) \quad (11)$$

Using a simple algebraic rearrangement, the term $(1 - e^{-2\gamma x})$ in equation (5) can be substituted to give an integral form because x is the distance in the z direction:

$$A = T^0 e^{-2\gamma x} + 2\gamma T^0 \int_0^x e^{-2\gamma z} dz \quad (12)$$

This may be re-written explicitly for each polarization by substituting equations (7) and (8) to yield the following:

$$A_p = \frac{2\gamma \operatorname{Re}[\hat{n}_2 \cos \hat{\theta}_2] |\hat{t}_p|^2}{n_1 \cos \theta_1} \int_0^x e^{-2\gamma z} dz \quad (13)$$

$$A_s = \frac{2\gamma \operatorname{Re}[\hat{n}_2 \cos \hat{\theta}_2] |\hat{t}_s|^2}{n_1 \cos \theta_1} \int_0^x e^{-2\gamma z} dz \quad (14)$$

An intrinsic assumption in this approach is that back reflection does not occur after the substrate, which neglects the term $T^0 e^{-2\gamma x}$ in equation (12), and is valid when there is no abrupt change in the real part of the refractive index. Equations (13) and (14) allow the exact calculation of absorptance (A) knowing an extinction coefficient profile for attenuated internal reflection. However, it is the aim of this paper to recover the concentration profile of absorbers as a function of depth from the internal reflection element within the substrate material. It is virtually impossible to do this using the exact solutions presented in equations (13) and (14). To make this solution tractable, it is necessary to introduce the assumption that k is small, which allows the simplification of equations (13) and (14) in the following manner. It is only necessary to make the following approximations if depth profile information is desired. Assuming k is small, and applying Snell's law, equation (2), the following simplifications can be made:

$$\operatorname{Re}[\hat{n}_2 \cos \hat{\theta}_2] \approx \frac{k(2n_1^2 \sin^2 \theta_1 - n_2^2)}{n_1 n_2 \sqrt{\sin^2 \theta_1 - \left(\frac{n_2}{n_1}\right)^2}} \quad (15)$$

$$\operatorname{Re}[\hat{n}_2 \cos \hat{\theta}_2] \approx \frac{n_2 k}{n_1 \sqrt{\sin^2 \theta_1 - \left(\frac{n_2}{n_1}\right)^2}} \quad (16)$$

$$|\hat{t}_p|^2 \approx \frac{(2n_1 \cos \theta_1)^2}{(n_2 \cos \theta_1)^2 + n_1^2 \left[\left(\frac{n_1}{n_2}\right)^2 \sin^2 \theta_1 - 1 \right]} \quad (17)$$

$$|\hat{t}_s|^2 \equiv \frac{(2n_1 \cos \theta_1)^2}{n_1^2 - n_2^2} \quad (18)$$

$$\gamma \equiv \frac{2\pi n_1 \sqrt{\sin^2 \theta_1 - \left(\frac{n_2}{n_1}\right)^2}}{\lambda} \quad (19)$$

Notice that the extinction coefficient, k , is shown with first order dependency because higher order terms have been neglected. For the situation where k is a function of z , this profile will fall under the integral shown in equations (13) and (14). The working equations for depth profile calculations are found by substituting the approximations shown in equations (15)-(19) into equations (13) and (14), as shown in equations (20) and (21).

$$A_p = \left(\frac{4\pi}{\lambda \cos \theta_1} \right) \left(\frac{(2n_1^2 \sin^2 \theta_1 - n_2^2)}{n_1 n_2} \right) \left(\frac{(2n_1 \cos \theta_1)^2}{(n_2 \cos \theta_1)^2 + n_1^2 \left[\left(\frac{n_1}{n_2} \right)^2 \sin^2 \theta_1 - 1 \right]} \right) \int_0^{\infty} k(z) e^{-2\gamma z} dz \quad (20)$$

$$A_s = \left(\frac{4\pi}{\lambda \cos \theta_1} \right) \left(\frac{n_2}{n_1} \right) \left(\frac{(2n_1 \cos \theta_1)^2}{n_1^2 - n_2^2} \right) \int_0^{\infty} k(z) e^{-2\gamma z} dz \quad (21)$$

The integral in equations (20) and (21) is recognized as the Laplace transform of $k(z)$, the concentration profile, where the Laplace variable $s=2\gamma$. This Laplace transform relationship was first noted by Hirschfeld.⁷ Therefore, to determine the concentration profile it is necessary to calculate the inverse Laplace transform of $A(s)$, in other words to measure the absorptance, A , at different angles and then to take the inverse Laplace transform, \mathcal{L}^{-1} with the appropriate scaling relations as shown in equations (22) and (23).

$$k(z) = \mathcal{L}^{-1} \left\{ \left(\frac{\lambda \cos \theta_1}{4\pi} \right) \left(\frac{n_1 n_2}{2n_1^2 \sin^2 \theta_1 - n_2^2} \right) \left(\frac{(n_2 \cos \theta_1)^2 + n_1^2 \left[\left(\frac{n_1}{n_2} \right)^2 \sin^2 \theta_1 - 1 \right]}{(2n_1 \cos \theta_1)^2} \right) A_p(s) \right\} \quad (22)$$

$$k(z) = L^{-1} \left\{ \left(\frac{\lambda \cos \theta_1}{4\pi} \right) \left(\frac{n_1}{n_2} \right) \left(\frac{n_1^2 - n_2^2}{(2n_1 \cos \theta_1)^2} \right) A_s(s) \right\} \quad (23)$$

It is encouraging that equation (23) is identical to the result obtained by Tompkins⁸ after making the proper substitutions to calculate k , and adding the term for the initial field from the Fresnel transmission coefficient, equation (18), which was not shown explicitly in his work. Previous attempts to determine concentration profiles by Reichert et al⁹. and Fina et al.¹⁰ were done using perpendicularly polarized light or by neglecting polarization as in Popov et al.¹¹

The theory assuming small k will be checked by comparison with the exact solution of the absorptance from the complex refractive index based on Fresnel's relations. The numerical solution compares perfectly with the matrix formalism presented by Hansen³ as well as the somewhat different approach used by Ohta et al.⁵ The complex refractive index for a model material was calculated from classical dispersion theory.¹² The complex dielectric constant, which is representative of any vibrational modes including electronic transitions, is expressed as:

$$\hat{\epsilon}(v) = \epsilon_\infty - \frac{(\epsilon_0 - \epsilon_\infty)v_0^2}{v^2 + i\zeta v - v_0^2} \quad (24)$$

where ϵ_0 and ϵ_∞ are the dielectric constants at $v=0$ and ∞ respectively. The damping coefficient for the oscillator is ζ , and v_0 is the frequency of the proper vibration. The complex refractive index is the square root of the complex dielectric constant for dielectric materials, where the magnetic permeability is unity.

$$\hat{n}(v) = \sqrt{\hat{\epsilon}(v)} \quad (25)$$

The use of classical dispersion theory to obtain model optical constants free from error is used to determine the errors involved with the approximations given in equations (15) - (19). This procedure has been shown to have great utility in previous studies.¹³ Using the approximations outlined in the theory section, it is evident that the real part of the refractive index must be constant. Of course, this is not strictly valid during an absorption, since the real and imaginary components are bound by a Kramer's-Kronig relation, i.e. causality. Therefore, the primary use

of the classic damped oscillators is to determine the effect of neglecting the optical dispersion. The effects of optical dispersion will be minimized with smaller extinction coefficients, therefore this approximation is commensurate with the previous assumptions.

Experimental:

The programs used to simulate spectra based on classical dispersion theory were written in Fortran77 on a MicroVAX II with a VMS operating system. The statistical fitting of the inverse Laplace transform was performed on a Macintosh using Systat® software which is commercially available.

This method requires a premeditated choice of concentration profile. Upon choosing a candidate profile, the specific parameters of the model are determined and the overall model is evaluated statistically. For this paper, step profiles are simulated using the exact Fresnel solution, then the profile information is recovered using the approximate relations shown in equations (22) and (23). Both the film thickness and the estimate of the extinction coefficient will be compared to the original starting values.

Results:

The extinction coefficient was assumed to be small to make the depth profile problem tractable, and to that end the approximate relations, equations (15) - (19), were employed. The consequence of using the approximate forms may be seen in the following figures. The decay coefficient, γ , indicates the distance over which the field decays to $1/e$ of its initial value. Of course, this distance will be shorter in the case of absorption. The error involved with neglecting absorption, i.e. the percent difference between equations (6) and (19), is shown in Figure 2. For this calculation, a frequency of 1000 cm^{-1} and an angle of 26° was used. The angle being considered is close to the critical angle and represents close to the largest error, just as the error

would be less further from the critical angle. Here, the error is about 7% for $k = 0.2$, a relatively strong organic absorption, and falls to zero as k tends toward zero.

The Fresnel transmission coefficient, $|\hat{t}|$, represents the initial field in medium 2 at zero depth. The error caused by neglecting the extinction coefficient, i.e. the percent difference between equations (9) and (17) for p-polarization, and (10) and (18) for s-polarization, is shown in Figure 3. Here the angle of incidence is 26° , close to the critical angle which is the condition for the largest error. The error is about 8% for $k=0.2$ using s-polarization, but is almost 3 times higher for p-polarization. Again, the error drops to zero as the extinctions coefficient tends toward zero.

The final set of approximations comes from the terms $\text{Re}[\hat{n}_2^* \cos \hat{\theta}]$, for p-polarization and $\text{Re}[\hat{n}_2 \cos \hat{\theta}]$ for s-polarization. These terms are assumed to behave first order with respect to k , and it is from these terms that the extinction coefficient profile is determined. The error in this assumption is obtained by comparing the directly calulated values with equations (15) and (16) for p-polarization and s-polarization, respectively. The results for an incident angle of 26° , one of the highest error conditions, are shown in Figure 4. Here the error for the parallel component is lower, about half that of the perpendicular component. The error for p-polarization is about 4% for a $k=0.2$.

To a first approximation, best results would be obtained by considering s-polarization, in particular because the error in the Fresnel transmission coefficient is very high for p-polarization. However, p-polarization is attractive because it has a lower error for the term $\text{Re}[\hat{n}_2^* \cos \hat{\theta}]$. Therefore, it may be possible to make better use of p-polarization by iterating. Indeed, this procedure will reduce the error for both polarizations, but the effect will be more profound for p-polarization. The iterations would involve taking the estimate of k from the first approximation, and returning this value to calculate a refined estimate for the Fresnel transmission coefficient and decay constant. While this is possible, it will simply extend the usefulness of these developments, and both s and p polarizations may be used to determine depth profiles without

iterating, but p-polarization will be more sensitive to the extinction coefficient. The following section will illustrate the degree to which one can determine step profiles for both polarizations without iterating, and some examples of the benefits of iterating will be shown in the final section.

The preceding figures illustrate the degree of error imposed by the small extinction coefficient approximations. One major effect has not yet been explored, and that is the effect of optical dispersion, that the real and imaginary parts of the refractive index are coupled through a Kramer's-Kronig relation. To evaluate all of the effects simultaneously, model spectra were simulated using classical damped oscillators, equations (24) and (25), which follow Kramers-Kronig relations. Exact spectra were simulated for internal reflection at angles between 26 and 64° at half degree increments. The approximate relations were applied to these exact spectra, equations (22) and (23), and the extracted results were compared with the known input. For step profiles, the main variables are thickness and extinction coefficient, but these are also determined for different absorption frequencies.

By proper choice of the damping coefficients, it is possible to obtain spectra like that shown in Figure 5. A peak is placed at every 500 cm^{-1} between 3000 and 500 cm^{-1} . Here the extinction coefficient intensity is maintained at 0.05, but by changing ζ , it is possible to obtain other values. Consideration will also be given to $k=0.005$ and $k=0.5$. This allows the differentiation between weak, moderate, and strong organic absorptions.

Step profiles have a particularly simple Laplace transform. When $k(z)$ is a unit step of thickness t , directly from the optically dense material, then:

$$\int_0^{\infty} k(z) e^{-2\gamma z} dz = k \left(\frac{1 - e^{-\gamma t}}{\gamma} \right) \quad (26)$$

Here, the Laplace variable $s=2\gamma$, and this relation can be directly substituted into equations (20) and (21) for non-linear fitting in Laplace space. While the extinction coefficient is allowed to vary, the real part of the refractive index is not. Even after the step profile, the real part of the refractive index must be maintained. For a complex refractive index such as that shown in

Figure 5, this means that a transparent backing layer with $n = 1.5$ must be applied behind the stepped layer. A typical result of this non-linear fitting is shown in Figure 6. In this figure, a simulated result of a $0.5 \mu\text{m}$ thick film for different angles is shown with $k=0.05$ on germanium ($n=4.0$) at 1000 cm^{-1} using s-polarization. The solid line shows the best fit line using equations (21) and (26), returning an estimate for the thickness of $0.485 \mu\text{m}$ with an estimate for the extinction coefficient of 0.050, which corresponds to a 3% error in thickness and a negligible error for k .

For similar conditions, s-polarization at 1000 cm^{-1} on germanium, except here the thickness and the extinction coefficient are changed, the results are shown in Figure 7 and 8 respectively. For small absorptions, $k=0.005$, the estimated thickness remains less than 1% of the actual thickness to $2.0 \mu\text{m}$. For a moderate absorption, $k=0.05$, the error of the estimated thickness increases to 6.5 % for an actual thickness of $1.5 \mu\text{m}$. For a strong absorption, $k=0.5$, the errors are 20% or larger throughout the range of investigated thicknesses. The limit to the small k assumption depends on the level of tolerable error, but absorptions which are considered strong on the organic level are probably not desirable. The error in the estimated extinction coefficients are much lower. For weak and moderate absorptions, the error in k is practicably negligible, although it is definitely not negligible for a strong absorption. The error for a strong absorption is seen to decrease as the actual thickness is increased. Doing this increases the error in the estimated thickness, however the error for the estimated extinction coefficient drops because the exponential term in equation (26) is tending toward zero, making k the only parameter to be estimated.

For higher frequencies the trends are similar, however the overall error is higher for the estimated thickness, and lower for the extinction coefficients, as shown in Figures 9 and 10 respectively. The error for a small absorption, $k=0.005$, is up to 5% for $2 \mu\text{m}$ actual thickness, and for a moderate absorption, $k=0.05$, the error is at 10% for $1 \mu\text{m}$ actual thickness. The error in the estimated extinction coefficient is dramatically lower for the case of strong absorption, $k=0.5$.

If an incident media is used with a lower refractive index, for instance KRS-5 ($n=2.37$), then there is an even greater dependence on the extinction coefficient, as shown in Figures 11 and 12. The level of error in the estimated thickness and extinction coefficient is higher than the equivalent condition for germanium in all cases. In Figure 12, there is a curvature in the error for the estimated extinction coefficient for the actual extinction coefficient of 0.05. This is evident in all of the graphs showing $k=0.05$, however it is even more pronounced in Figure 12. Presumably this is because the effects of k and distance are well matched at the lowest error, while extinction dominates for thinner and distance dominates for thicker layers. For smaller k , the thickness dominates, and for larger k , the extinction dominates. Therefore, at large k it is difficult to determine layer thickness but easier to determine k . At small k , it is easy to determine layer thickness, and harder to determine k , even though the estimate of k is very good since our assumptions are most valid here. For moderate k , there is more evident a trade-off between these considerations.

The importance of maintaining a backing layer with the same refractive index is illustrated in Figures 13 and 14. Here, $k = 0.005$, s-polarization is used with 1000 cm^{-1} on KRS-5. The estimated thickness is shown in Figure 13. By abruptly changing the real part of the refractive index, from 1.5 for the layer to 1.0 for the backing material, there is a linear offset in the estimated thickness which is quite appreciable. Therefore, these abrupt changes in the real part of the refractive index are to be avoided. Fortunately, from an experimental consideration, most organic materials have their real part of the refractive index close to 1.5. The estimate of k also suffers a great deal until the sample thickness becomes thick enough that the backing layer becomes obscured.

When p-polarization is used, with 1000 cm^{-1} on germanium, the results are shown in Figures 15 and 16. The errors are consistently higher than that for the identical case with s-polarization. Of course, this increase in error was somewhat expected because the error in the Fresnel transmission coefficient, $|t|$, is significantly higher for p-polarization than for s-

polarization, as shown previously in Figure 3. It is possible to compensate for this error somewhat by using the estimate for k , and calculating a refined value of γ and $|\hat{t}|$, using equations (6) and (9) respectively. The results of this 2nd approximation are shown in Figures 17 and 18. The errors are drastically reduced at larger thicknesses. Interestingly, the errors are higher for thin layers. The approach which has been outlined inherently neglects optical dispersion. However, one of the effects of optical dispersion is to allow appreciable back reflection from the far side of the film when the film is sufficiently thin. Therefore, it is this effect which has become apparent and is causing the increased error for thin films in Figures 17 and 18. A back reflection allows additional absorption by increasing the actual field strength. This in turn causes the calculated thickness to be over-estimated because only the forward field is considered which then causes the field to be under-calculated. The extinction coefficient is estimated well in either case. For the first approximation, the field is set too high since absorption is neglected, which causes the thickness to be underestimated. For thin films, this effect is opposite in direction to the tendency to overestimate the thickness when the 2nd approximation is considered. Since these two effects are fortuitously opposing, the thin film errors are not evident in the preceding figures when the field and decay constant are not refined.

Conclusions:

Approximations are made of the the exact equations describing generalized internal reflection spectroscopy. These approximate relations allow the determination of depth profile information for either s-polarization or p-polarization. The errors invoked by the approximation of a small extinction coefficient have been evaluated for different conditions. It was found that the least error was obtained using s-polarization with as high an optical density for the incident medium as possible, germanium for infrared studies. The results for p-polarization have inherently higher error than the corresponding results for s-polarization, primarily due to greater sensitivity of the Fresnel transmission coefficient to the extinction coefficient for p-polarization

than for s-polarization. These errors may be reduced for larger thicknesses by employing an iteration technique made possible by the exact optical equations.

Acknowledgements:

The authors would like to acknowledge the helpful discussions and insights obtained from Kiyoshi Yamamoto and Akio Masui. This work was in part sponsored by the Office of Naval Research.

References:

- 1 N.J. Harrick, *J. Optical Soc. America*, **55**, 851 (1965).
- 2 Eugene Hecht, "Optics," Addison-Wesley, Reading, Mass., 1987.
- 3 A. Masui, K. Yamamoto, and K. Ohta, *Bunseki Kagaku*, **41**, T49 (1992).
- 4 A. Masui and K. Yamamoto, *Private Communication*.
- 5 K. Ohta and H. Ishida, *Appl. Optics*, **29**, 1952 (1990).
- 6 W. Hansen, *J. Optical Soc. America*, **58**, 380 (1968).
- 7 T. Hirschfeld, *Appl. Spectrosc.*, **31**, 289 (1977).
- 8 H.G. Tompkins, *Appl. Spectrosc.*, **28**, 335 (1974).
- 9 W.M. Reichert, P.A. Suci, T. Ives, and J.D. Andrade, *Appl. Spectrosc.* **41** (3), 503 (1987).
- 10 L. Fina and G. Chen, *Vibrational Spectroscopy*, **1**, 353 (1991).
- 11 V.Y. Popov and V.V. Lavrent'ev, translated from *Zhurnal Prikladnoi Spektroskopii*, **32** (2), 336 (1980).
- 12 F. Wooten, "Optical Properties of Solids," Academic Press, New York, 1972.
- 13 K. Yamamoto, A. Masui, and H. Ishida, submitted to *Appl. Spectrosc.*

Figure 1: Schematic illustration the internal reflection arrangement.

Figure 2: % Error in the decay coefficient, γ , caused by neglecting the extinction coefficient. The conditions used for the calculation were 26° incidence and 1000 cm^{-1} .

Figure 3: % Error in the magnitude of the Fresnel transmission coefficient, $|t|$, for s-polarization (solid line) and p-polarization (dashed line) caused by neglecting the extinction coefficient calculated at 26°.

Figure 4: % Error in $\text{Re}[\hat{n}_2 \cos \hat{\theta}_2]$ for s-polarization (solid line) and in $\text{Re}[\hat{n}_2^* \cos \hat{\theta}_2]$ for p-polarization (dashed line) calculated at 26°.

Figure 5: Results of classic damped oscillators, k & n for substrate.

Figure 6: Simulated Absorptance (o) for $k=0.05$ spectra 0.5 μm thick on germanium at 1000 cm^{-1} with s-polarization. Solid line is best fit for step profile using approximate relations.

Figure 7: % Error in the estimated thickness for s-polarization at 1000 cm^{-1} on germanium.

Figure 8: % Error in the estimated k for s-polarization at 1000 cm^{-1} on germanium.

Figure 9: % Error in the estimated thickness for s-polarization at 2000 cm^{-1} on germanium.

Figure 10: % Error in the estimated k for s-polarization at 2000 cm^{-1} on germanium.

Figure 11: % Error in the estimated thickness for s-polarization at 1000 cm^{-1} on KRS-5.

Figure 12: % Error in the estimated k for s-polarization at 1000 cm^{-1} on KRS-5.

Figure 13: Estimated thickness for $n_{\text{backing}}=1.5$ and $n_{\text{backing}}=1.0$ for $k=0.005$, s-polarization at 1000 cm^{-1} on KRS-5.

Figure 14: Estimated k for $n_{\text{backing}}=1.5$ and $n_{\text{backing}}=1.0$ for $k=0.005$, s-polarization at 1000 cm^{-1} on KRS-5.

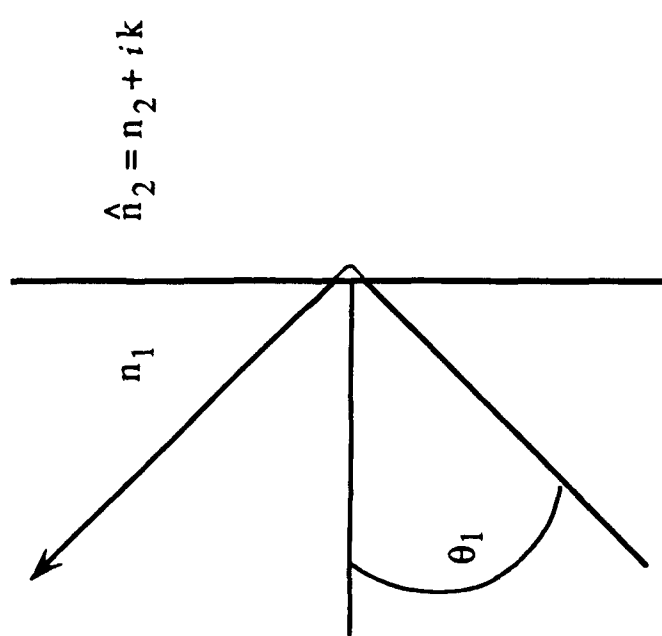
Figure 15: % Error in the estimated thickness for p-polarization at 1000 cm^{-1} on germanium.

Figure 16: % Error in the estimated k for p-polarization at 1000 cm^{-1} on germanium.

Figure 17: % Error in the estimated thickness for p-polarization at 1000 cm^{-1} on germanium to a 2nd approximation.

Figure 18: % Error in the estimated k for p-polarization at 1000 cm^{-1} on germanium to a 2nd approximation.

Figure 1



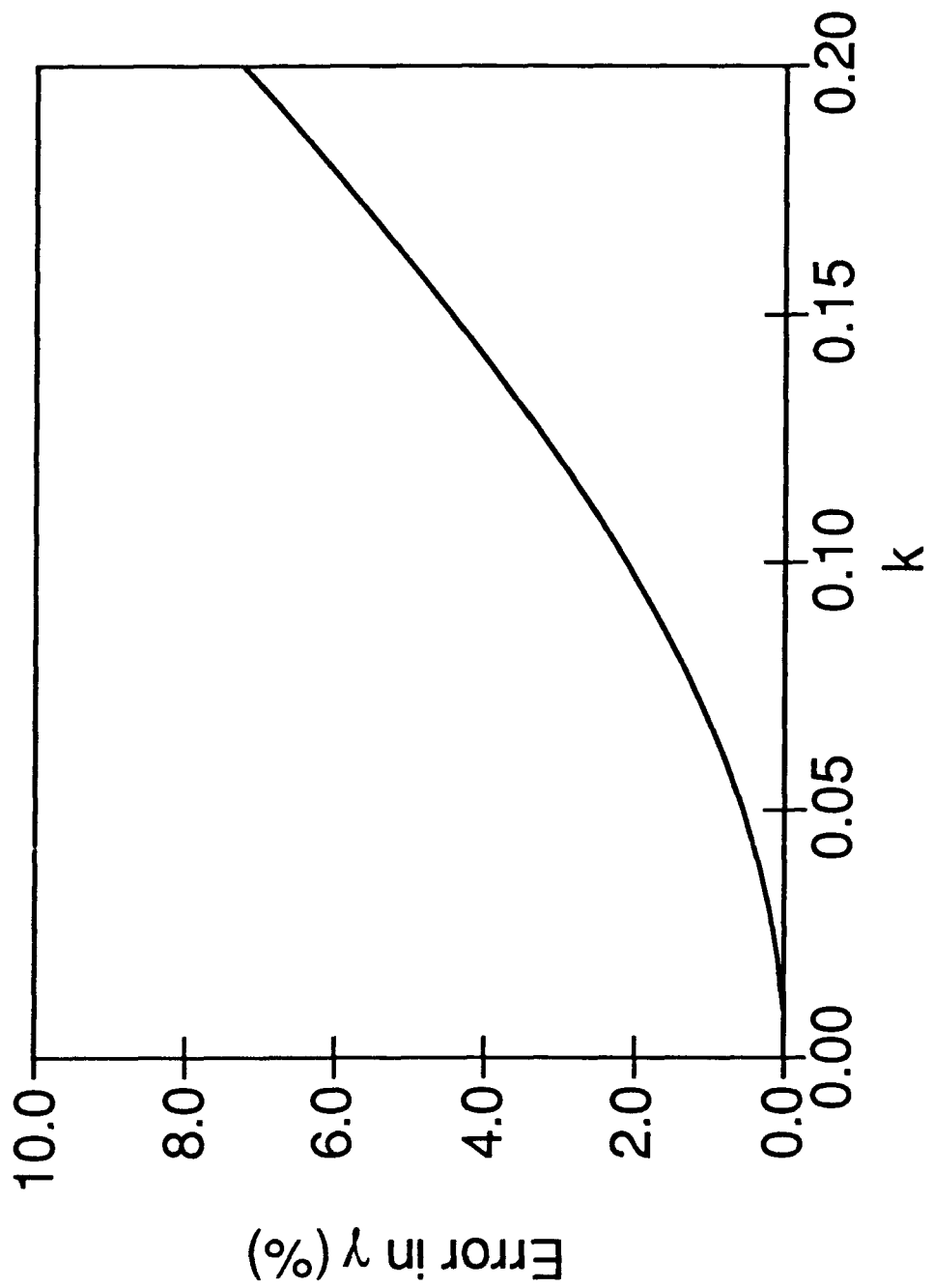


Figure 2

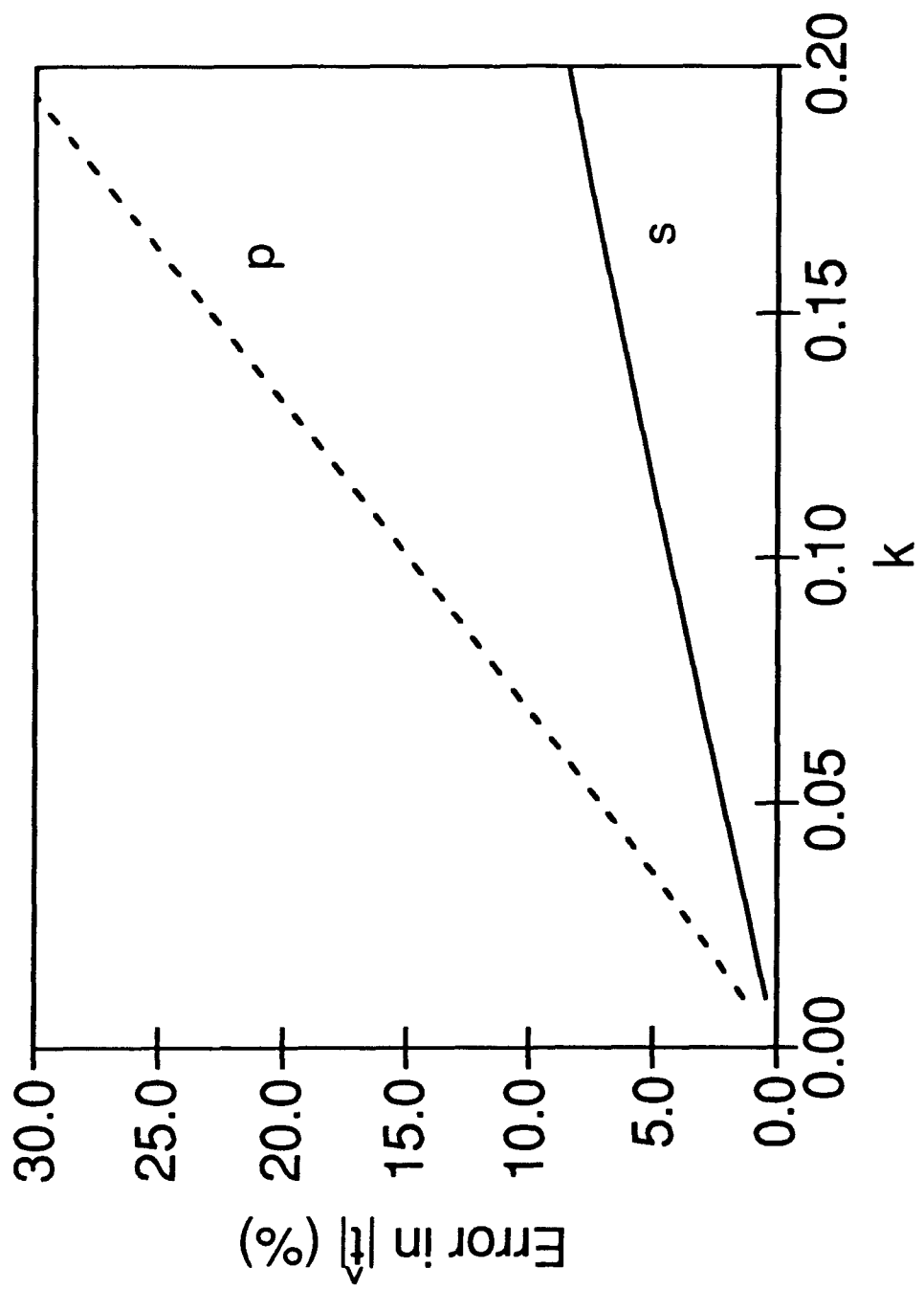


Figure 3

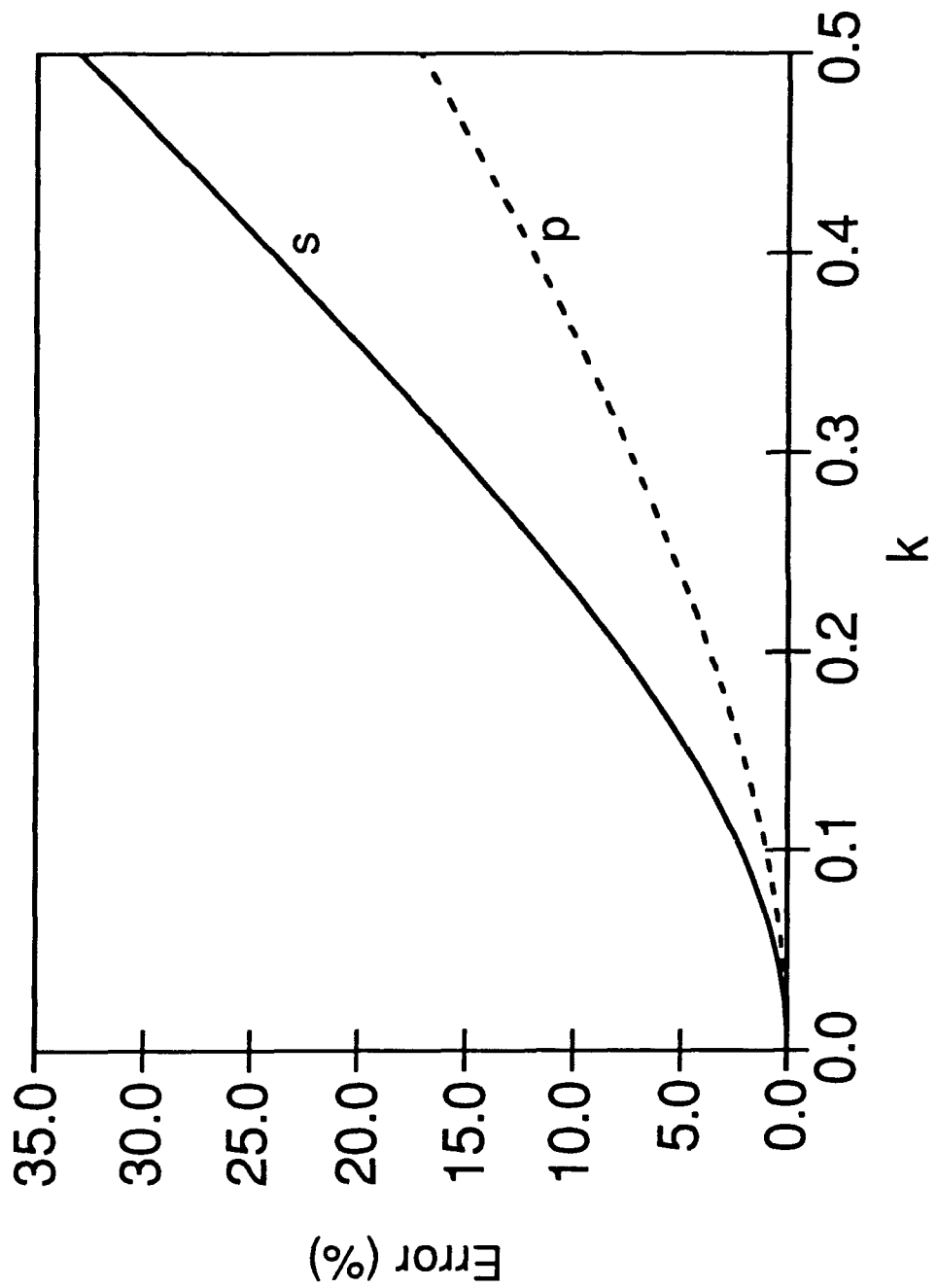


Figure 4

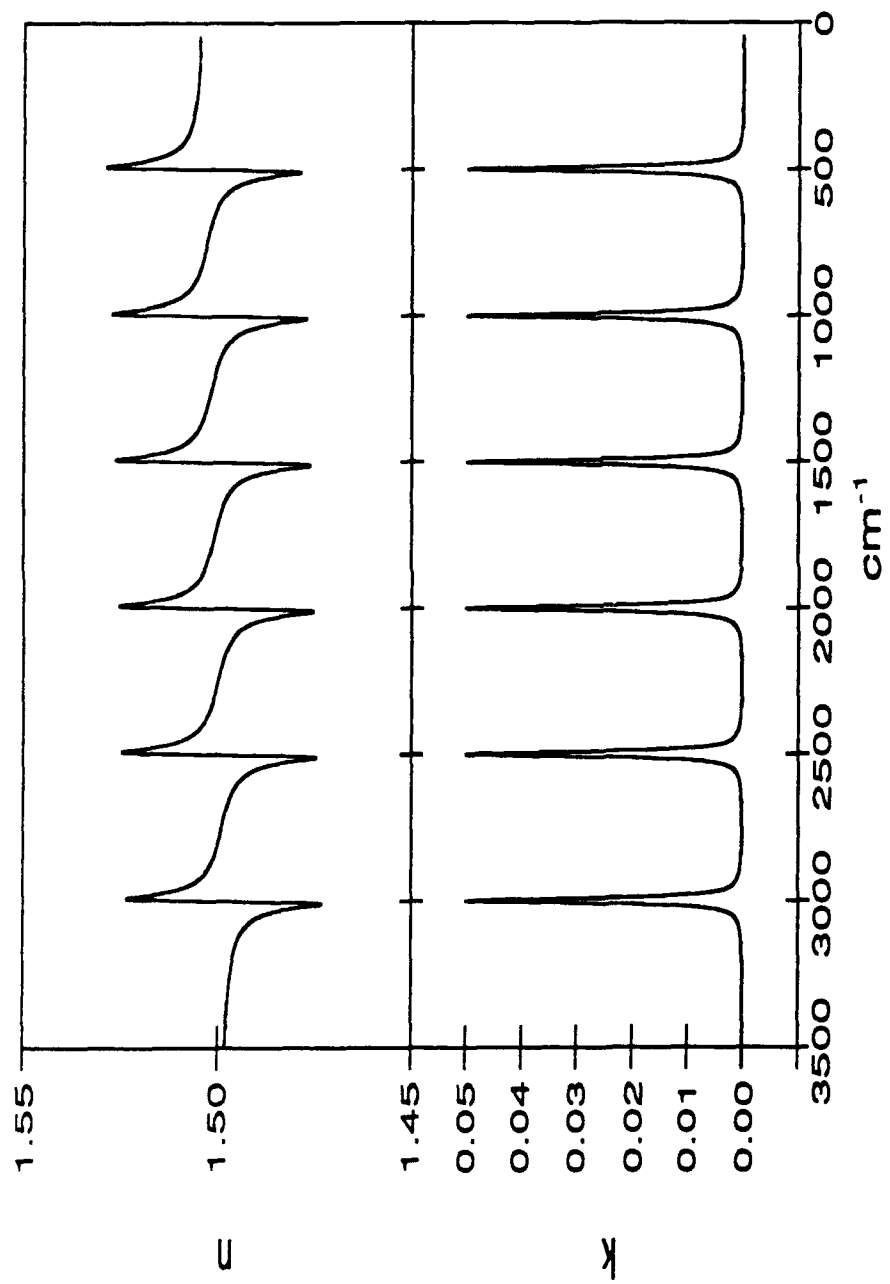


Figure 5

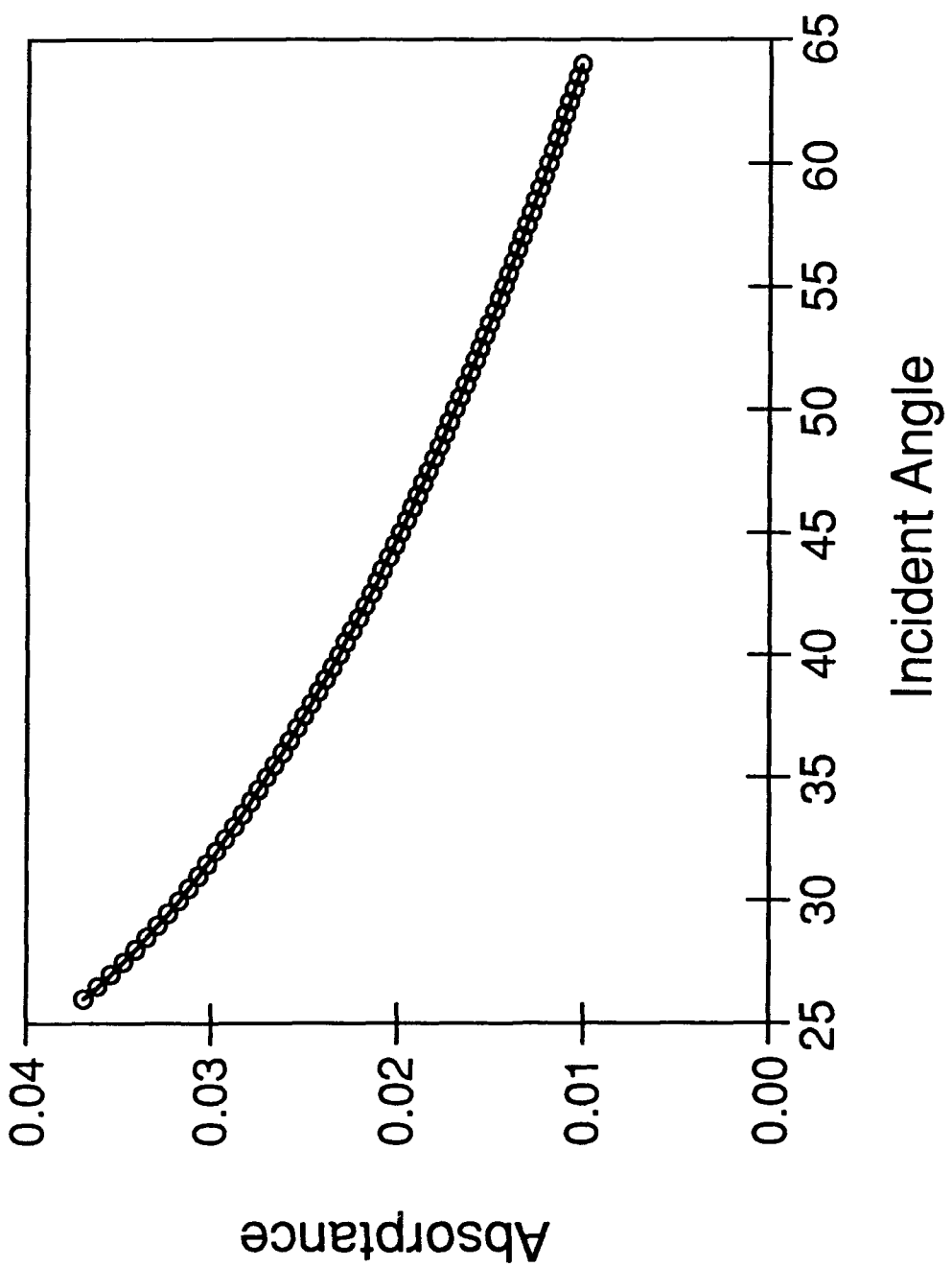


Figure 6

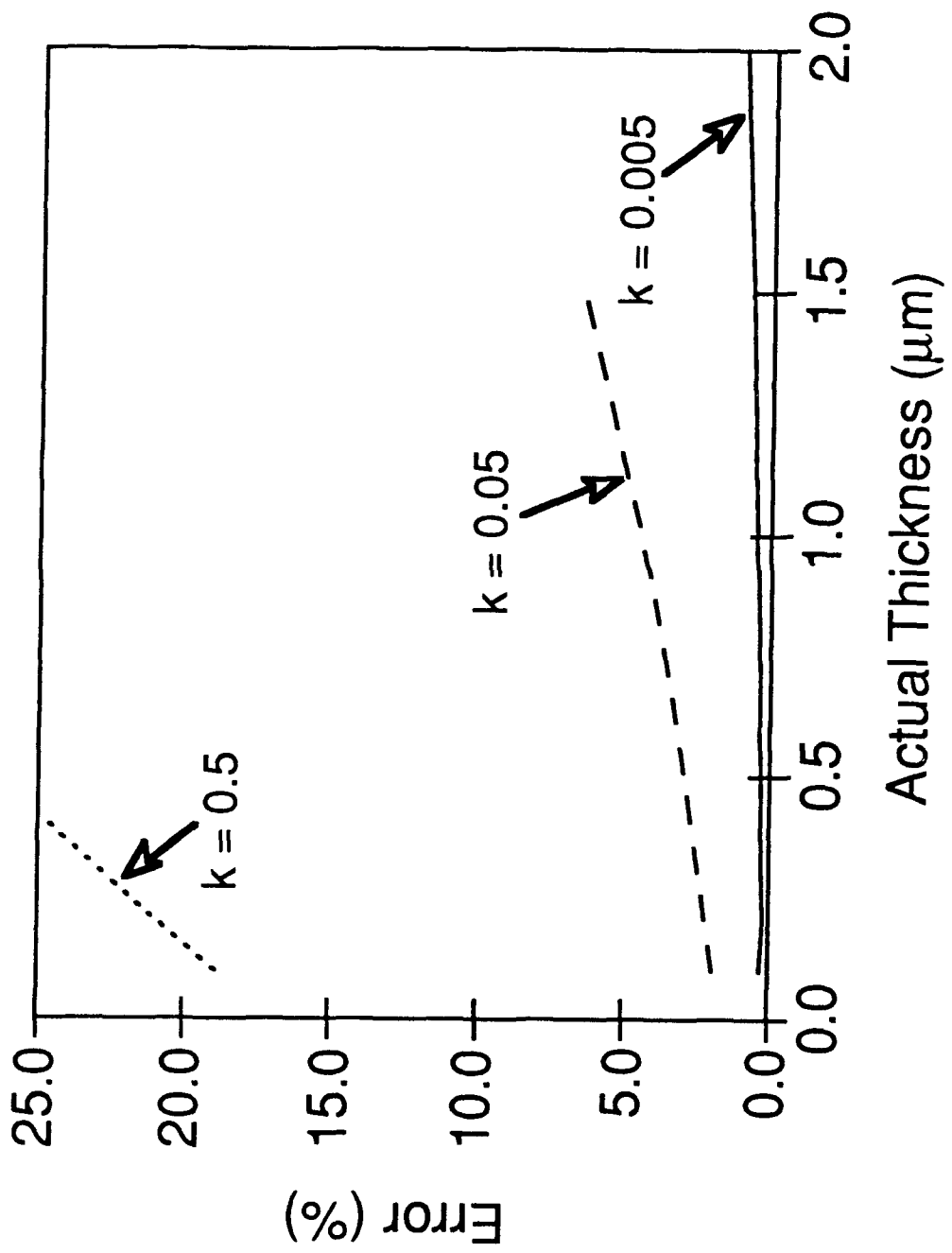


Figure 7

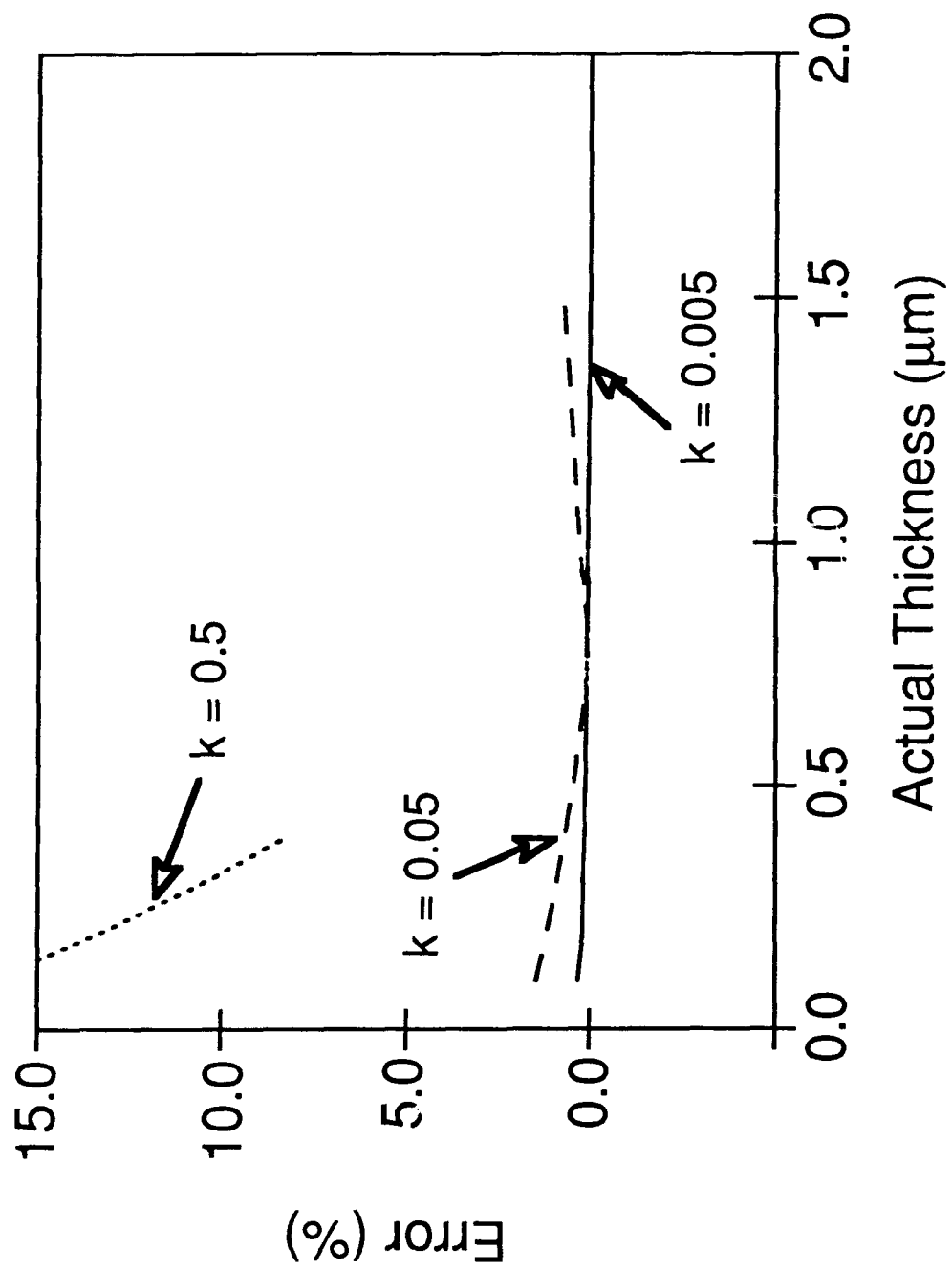


Figure 8

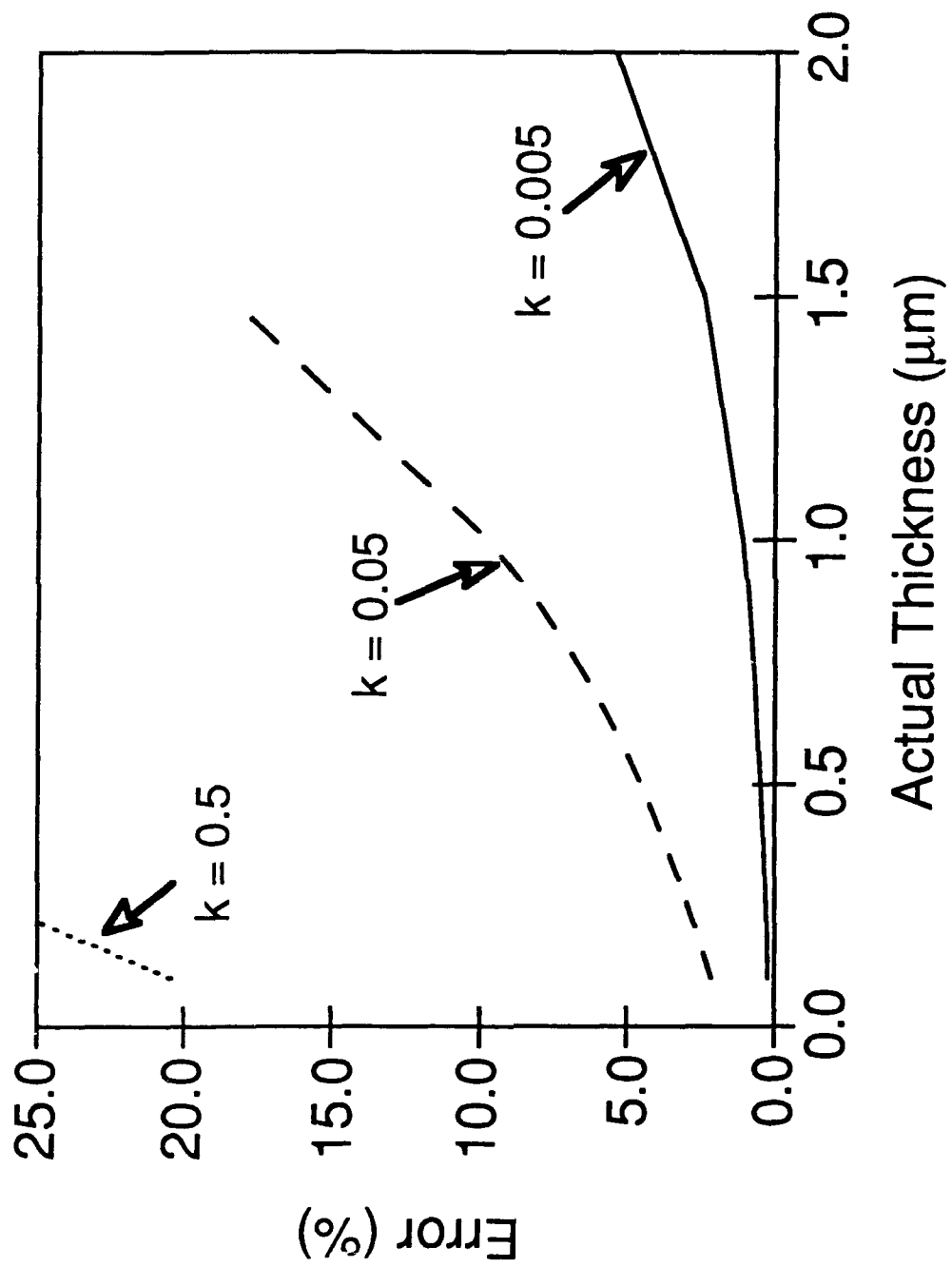


Figure 9

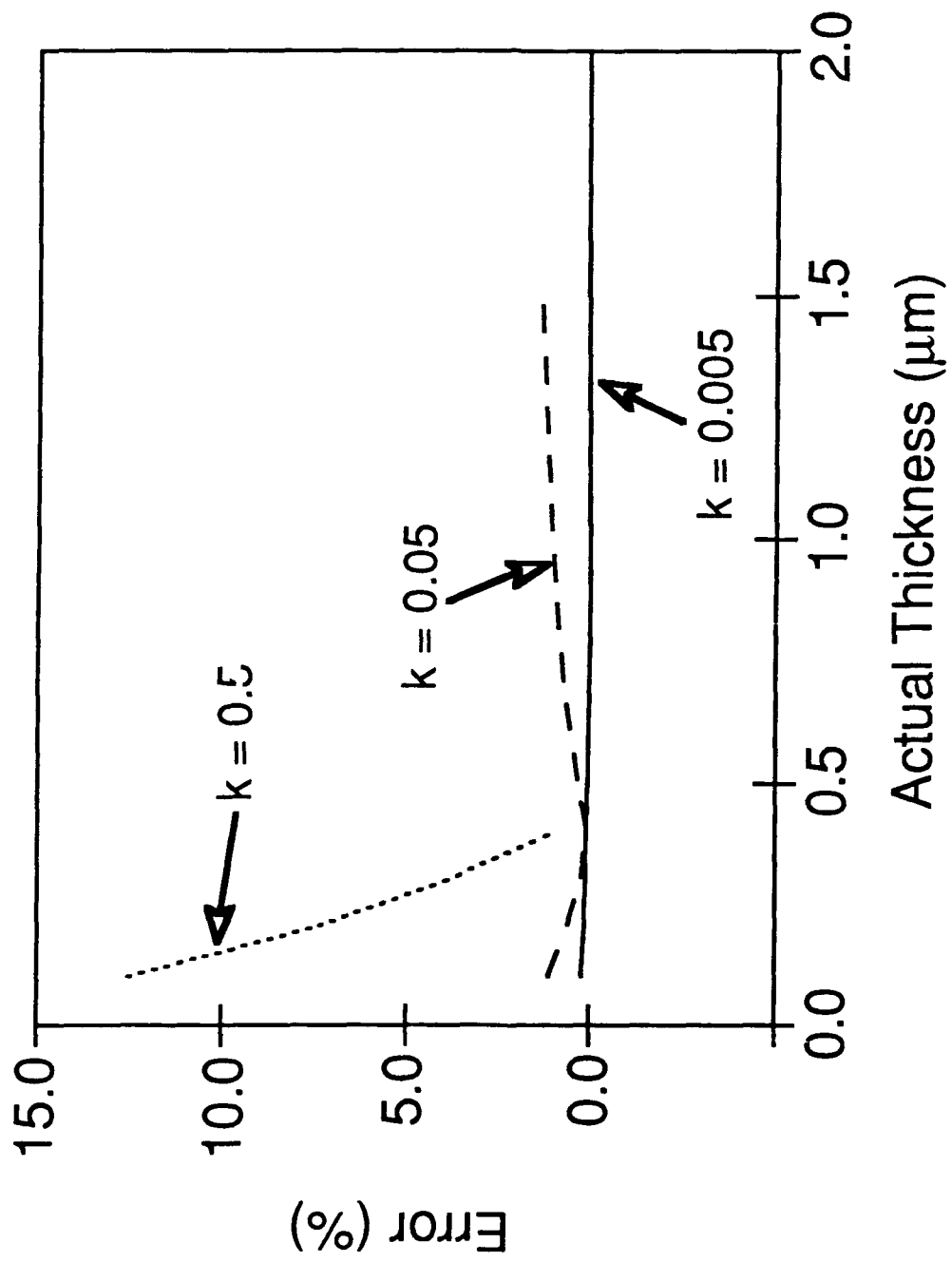


Figure 10

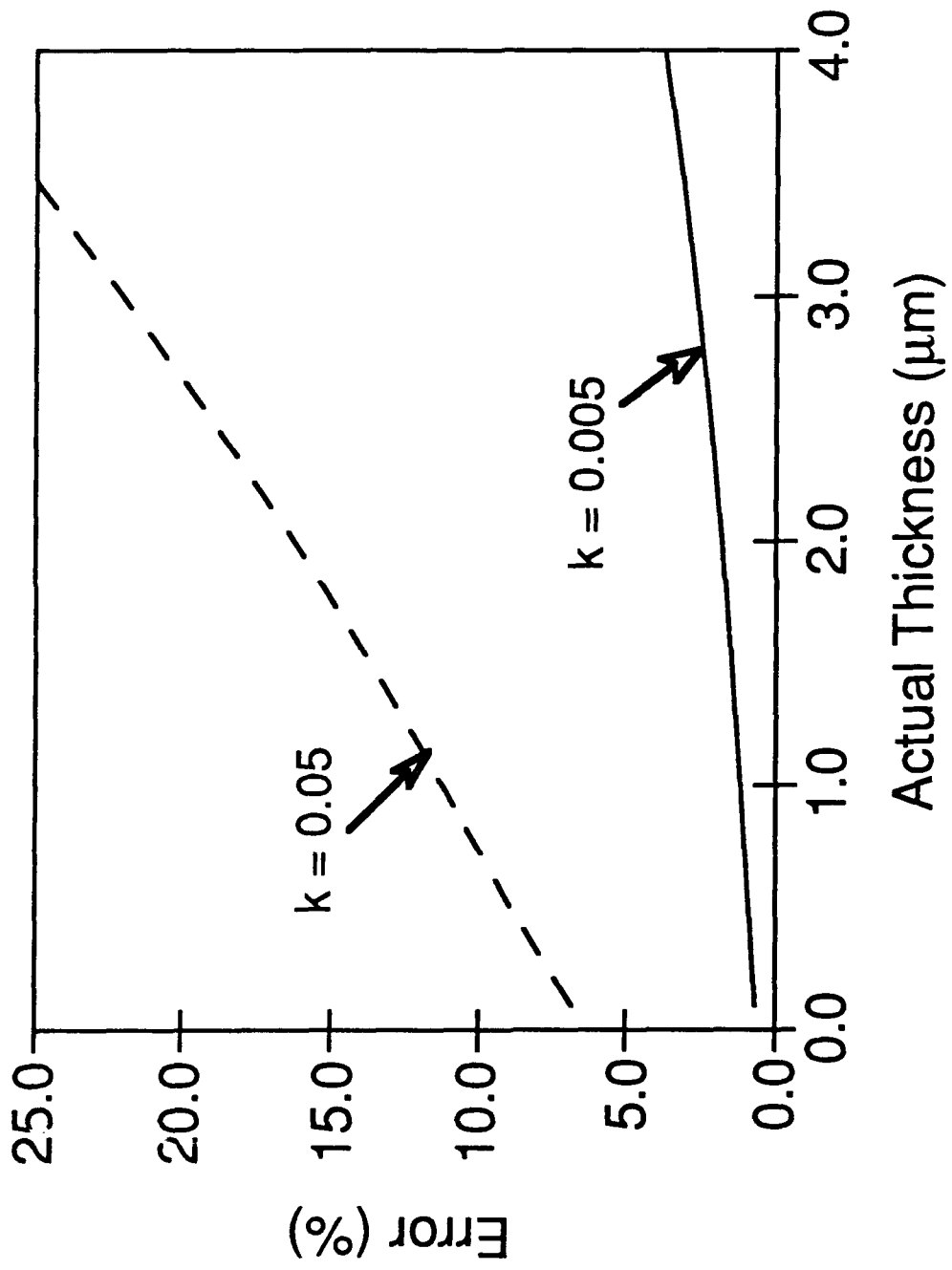


Figure 11

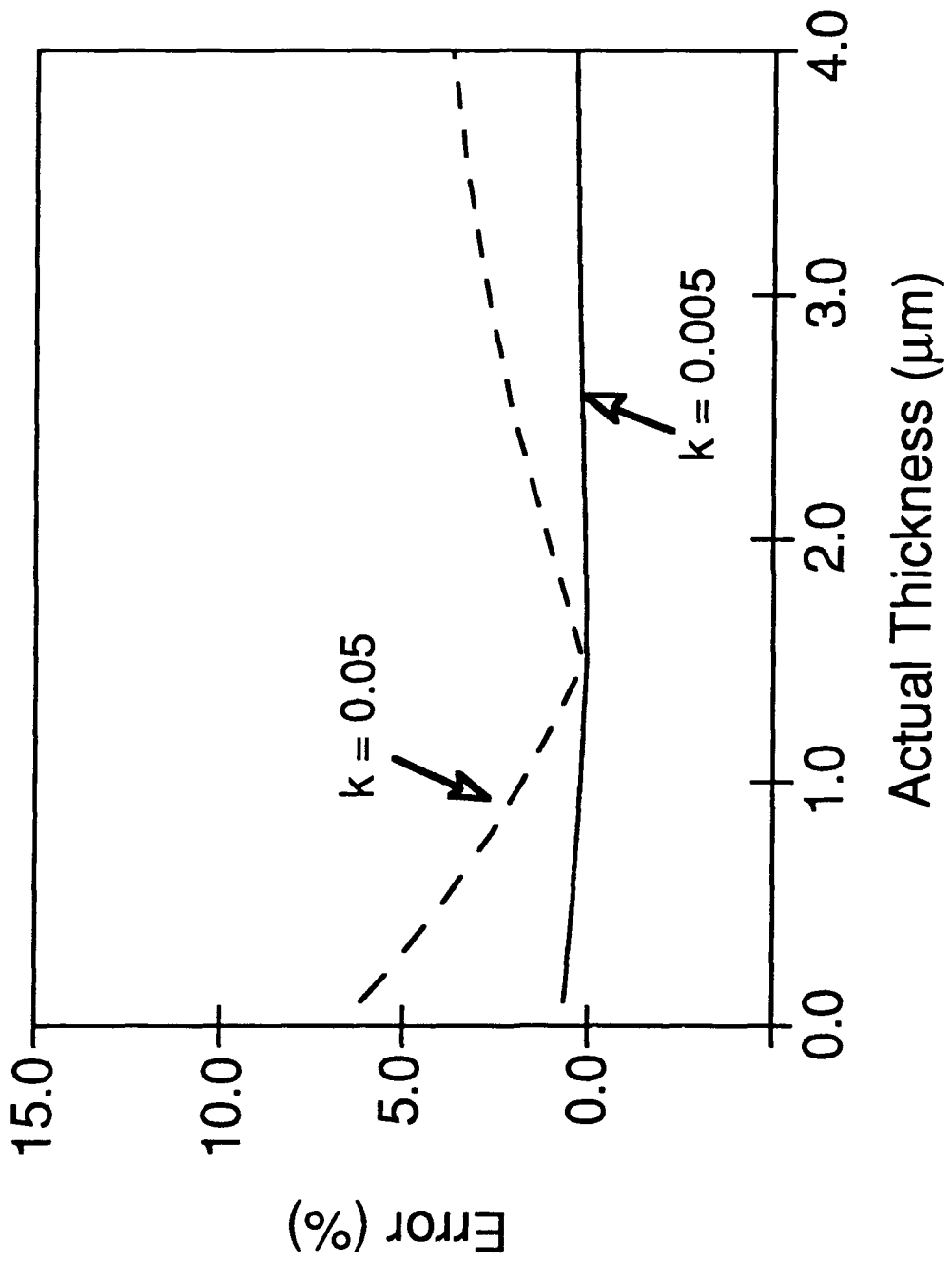


Figure 12

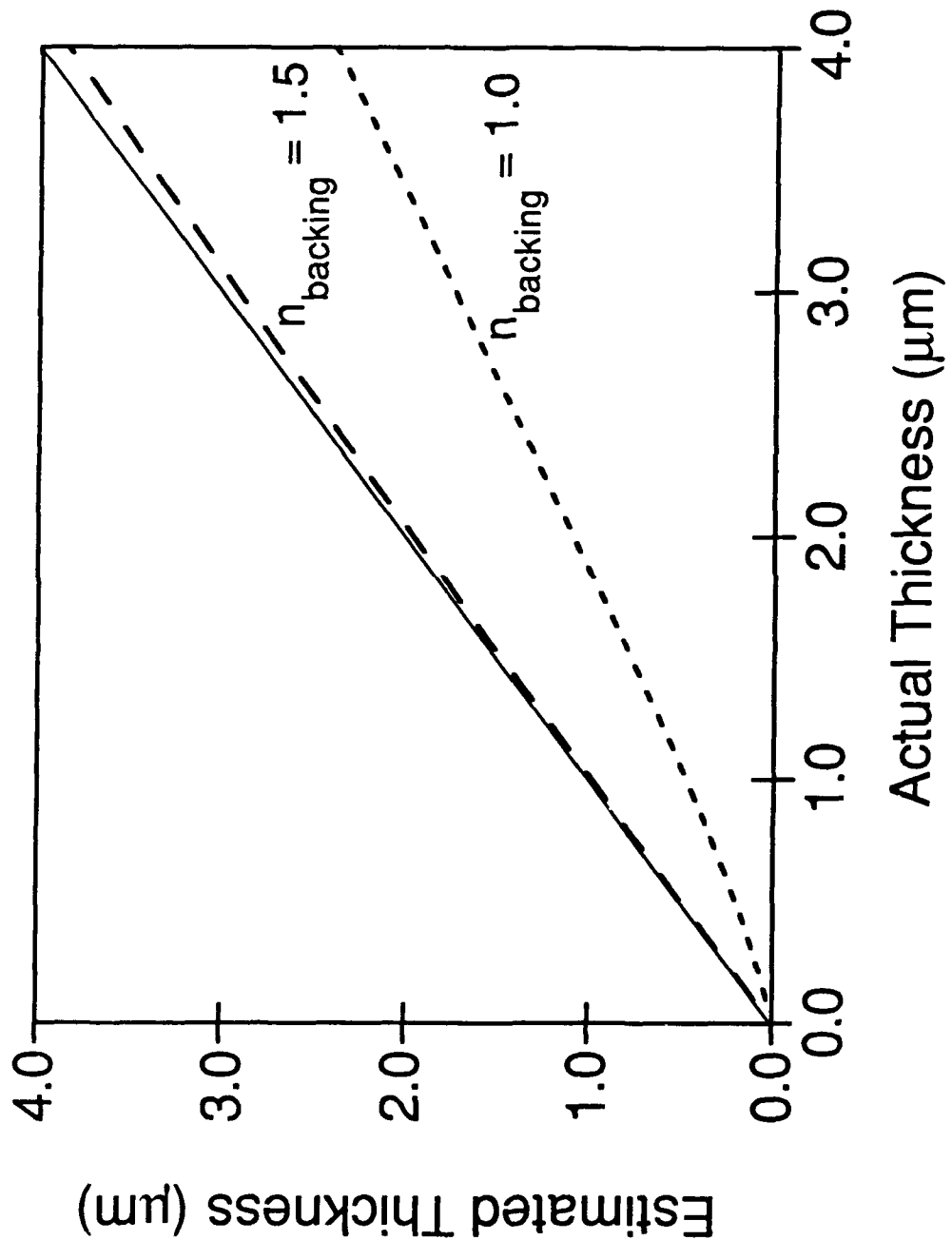


Figure 13

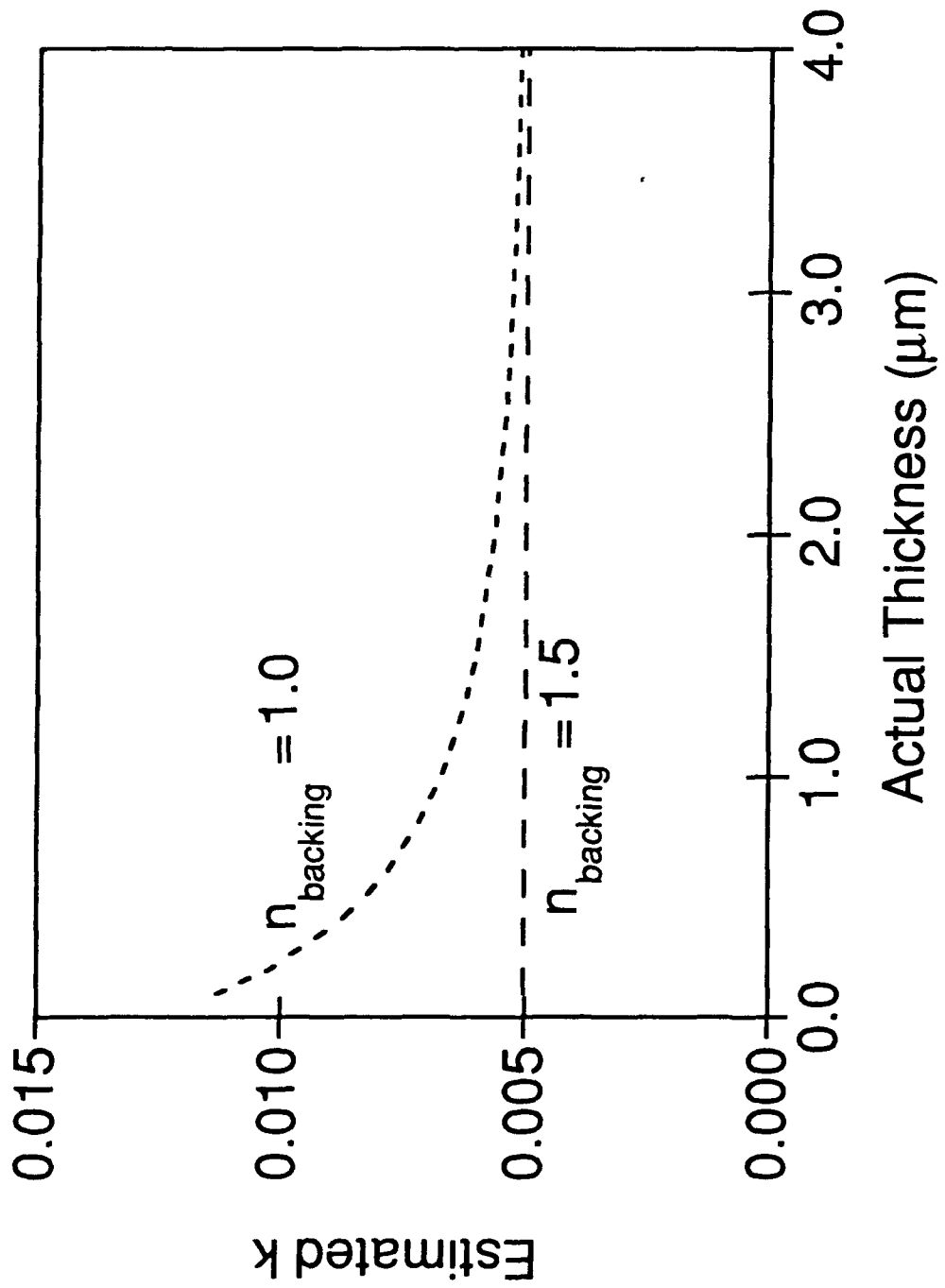


Figure 14

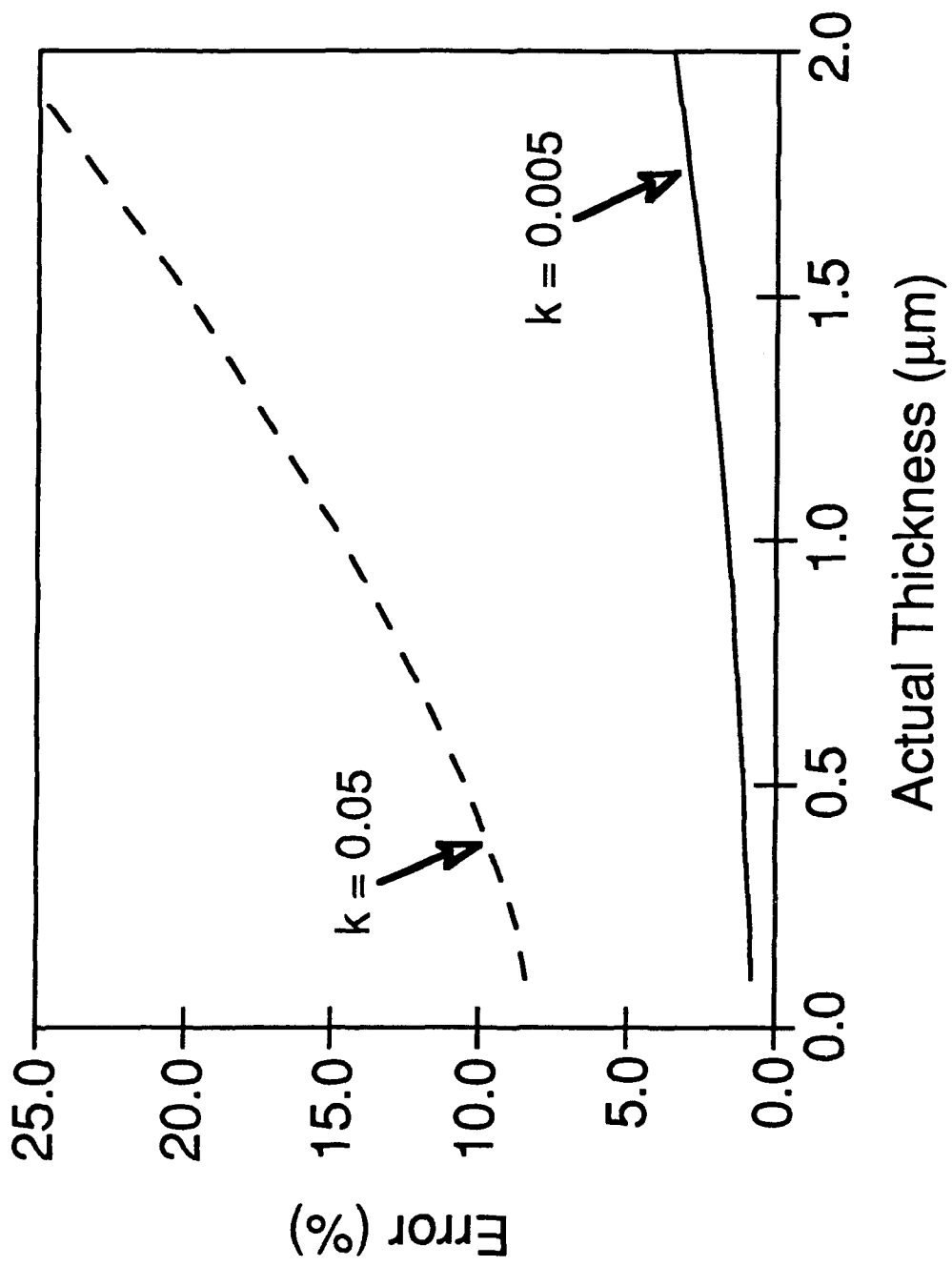


Figure 15

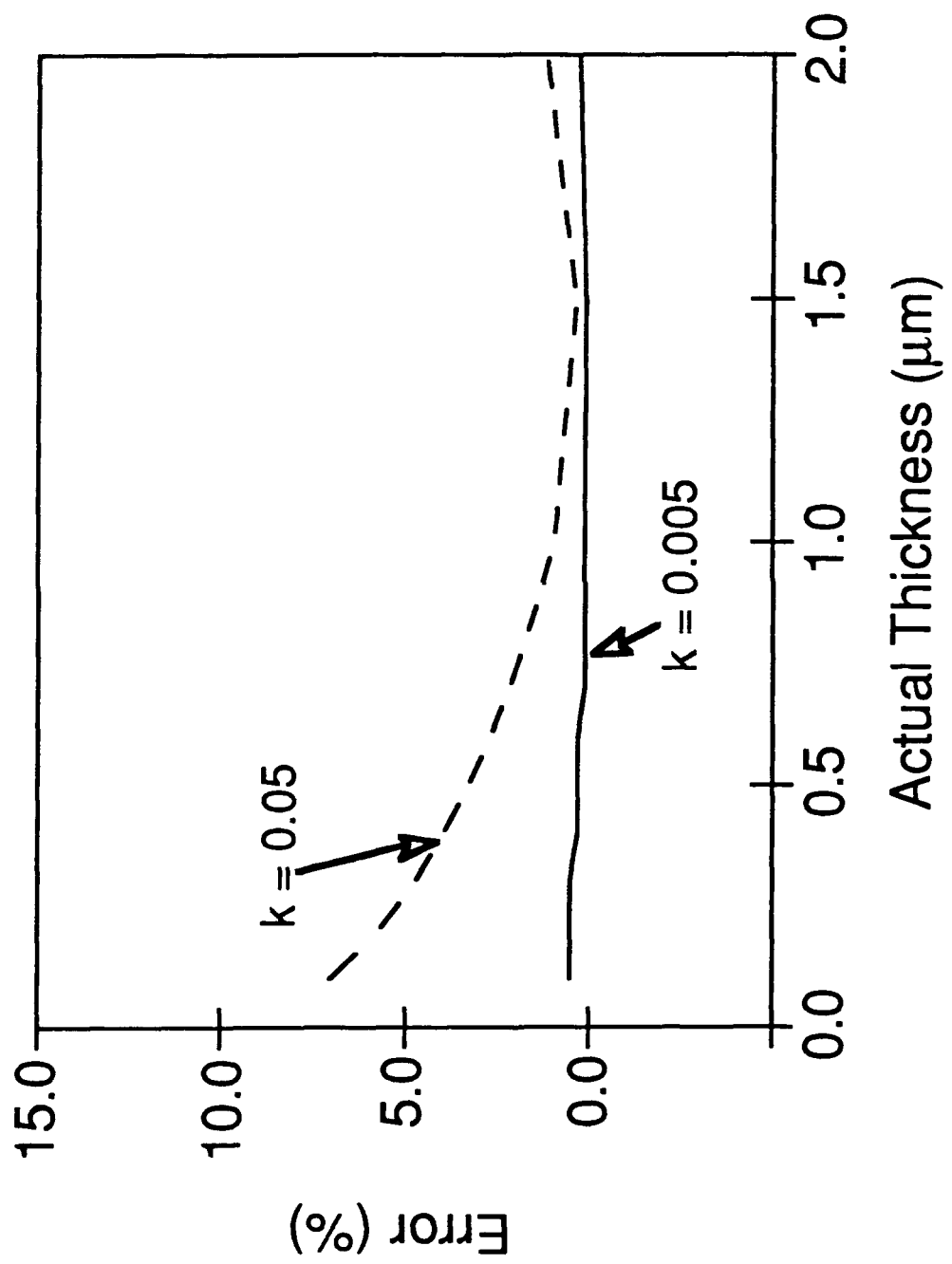


Figure 16

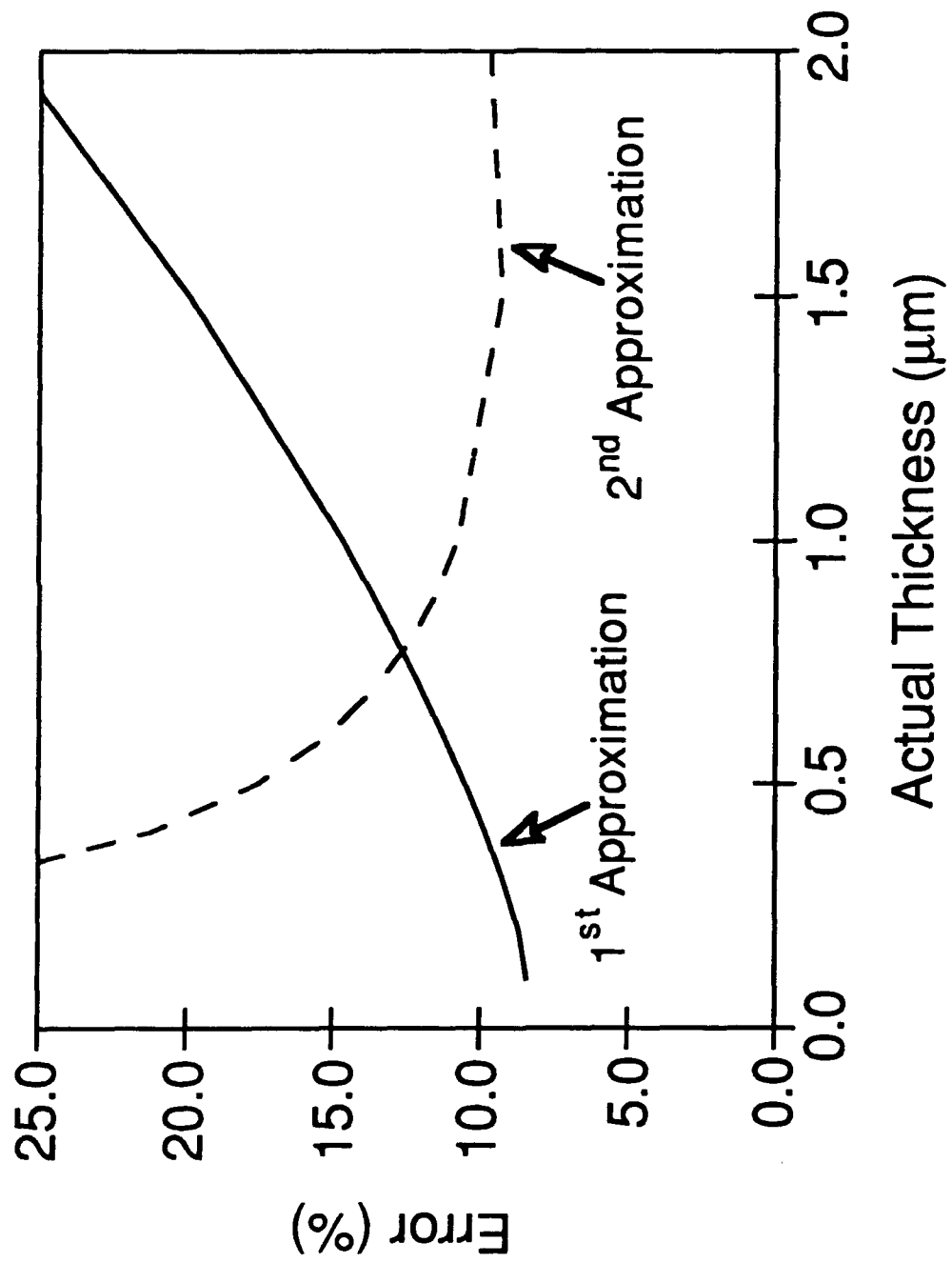


Figure 17

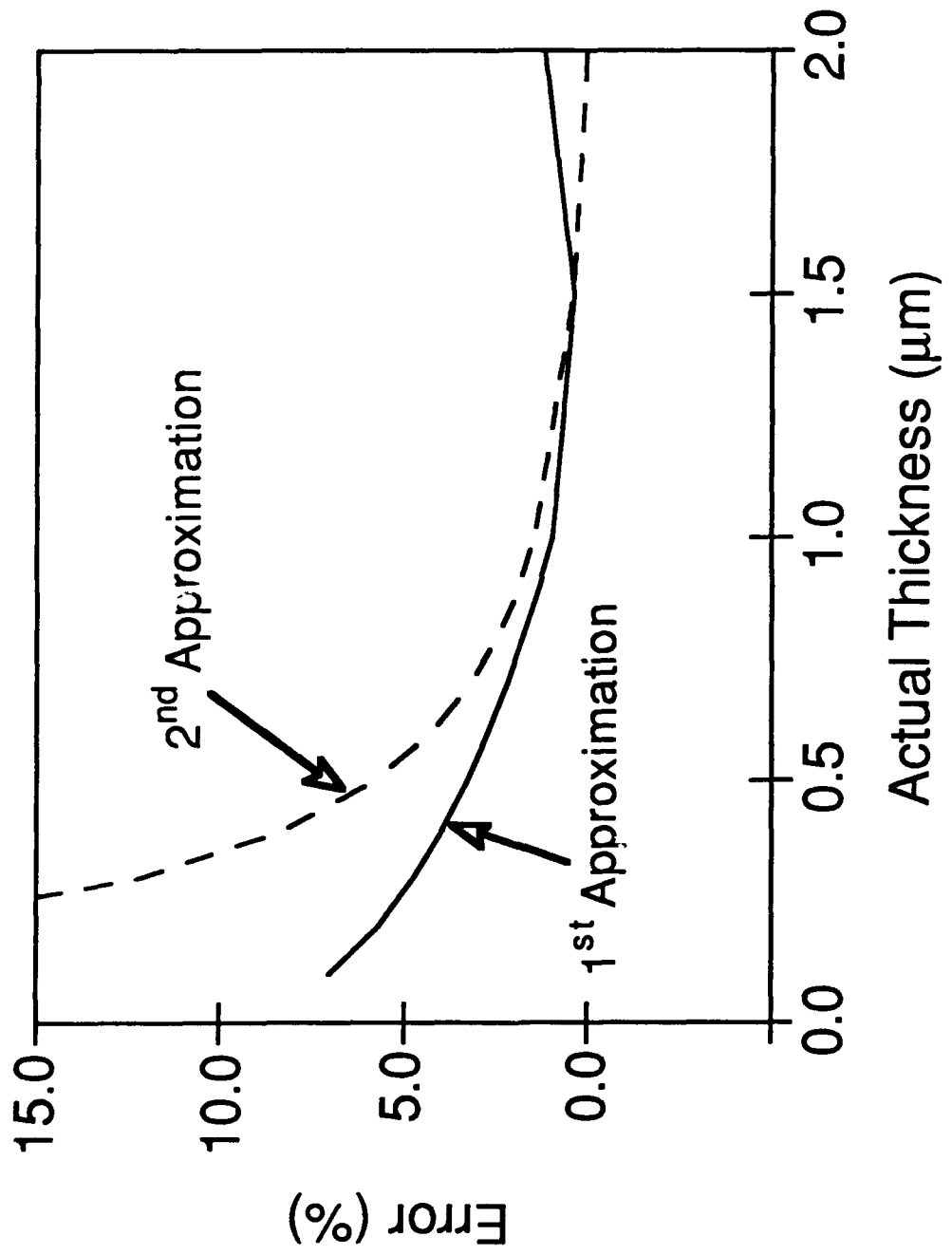


Figure 18